# THE SPECTRAL ELEMENT METHOD (SEM): FORMULATION AND IMPLEMENTATION OF THE METHOD FOR ENGINEERING SEISMOLOGY PROBLEMS

**Kristel C. Meza-Fajardo[1] and Apostolos S. Papageorgiou[2]**

[1]*Professor, Depto. de Ingenieria Civil,Universidad Nacional Autónoma de Honduras,Tegucigalpa, Honduras*
[2] *Professor, Department of Civil Engineering, University of Patras, GR-26500 Patras, Greece*
*Email: kcmeza@upatras.gr, papaga@upatras.gr*

## ABSTRACT

Various numerical methods have been proposed and used to investigate wave propagation in realistic earth media. Recently an innovative numerical method, known as the Spectral Element Method (SEM), has been developed and used in connection with wave propagation problems in 3D elastic media (Komatitsch and Tromp, 1999). The SEM combines the flexibility of a finite element method with the accuracy of a spectral method and it is not cumbersome in dealing with non-flat free surface and spatially variable anelastic attenuation. The SEM is a highly accurate numerical method that has its origins in computational fluid dynamics. One uses a weak formulation of the equations of motion, which are solved on a mesh of hexahedral elements that is adapted to the free surface and to the main internal discontinuities of the model. The wavefield on the elements is discretized using high-degree Lagrange interpolants, and integration over an element is accomplished based upon the Gauss-Lobatto-Legendre integration rule. This combination of discretization and integration results in a diagonal mass matrix, which greatly simplifies the algorithm. The most important property of the SEM is that the mass matrix is exactly diagonal by construction, which drastically simplifies the implementation and reduces the computational cost because one can use an explicit time integration scheme without having to invert a linear system. Furthermore, it allows an efficient parallel implementation. We sketch the formulation of the SEM in matrix form that is familiar to earthquake engineers. We demonstrate the efficiency and effectiveness of the method by implementing the proposed formulation to study various simple/canonical problems.

**KEYWORDS:** spectral element method, elastodynamics, elastic wave propagation, perfectly matched layer, engineering seismology

## 1. INTRODUCTION

Originally developed to address problems in fluid dynamics, the SEM combines the flexibility of a Finite Element Method (FEM) with the accuracy of a spectral method, allowing the computation of accurate synthetic seismograms in heterogeneous earth models with arbitrary geometry. The SEM is a highly accurate numerical method and it is not cumbersome in dealing with non-flat free surface and spatially variable anelastic attenuation. One uses a weak formulation of the equations of motion, which are solved on a mesh of hexahedral elements that is adapted to the free surface and to the main internal discontinuities of the model. The wavefield on the elements is discretized using high-degree Lagrange interpolants, and integration over an element is accomplished using the *Gauss-Lobatto-Legendre* (*GLL*) integration rule. This ensures minimal numerical grid dispersion and anisotropy. The most important property of the SEM is that the mass matrix is exactly diagonal by construction, which drastically simplifies the implementation and reduces the computational cost because one can use an explicit time integration scheme without having to invert a linear system. Furthermore, it allows an efficient parallel implementation.

The SEM was first introduced by Patera (1984) to solve problems of computational fluid dynamics. Its development was the result of combining the accuracy and rapid convergence of the pseudo-spectral methods with the geometrical flexibility of the FEM. Chebyshev polynomials were the basis polynomials for interpolation in the original work by Patera (1984). This choice was motivated by the fact that expansions with Chebyshev polynomials have the same

(exponential) convergence as Fourier series. Hence, the word *'Spectral'* in the SEM is related to the exponential convergence it achieves when the order of interpolating polynomials is increased.

An alternative to the Chebyshev SEM was developed by Maday and Patera (1989), with the use of a Lagrange interpolation in conjunction with the GLL quadrature, leading to a *diagonal* structure of the mass matrix. Adopting such approach, Komatitsch (1997) and Komatitsch and Vilotte (1998) applied the SEM to simulate wave propagation in large-scale 3-D structures. Exploiting the advantage of an *exactly* diagonal mass matrix, they implemented an explicit time scheme and achieved an effective parallel implementation.

For simulations related to wave propagation in unbounded domains, truncation of the domain is necessary, due to finite computational resources. An artificial boundary limiting the computational (or physical) domain is then introduced, and then boundary conditions must be specified so that the solution in the physical domain is an accurate representation of the solution in the unbounded domain. It turns out that devising such boundary conditions is by no means a trivial matter. The most common techniques implemented in wave propagation problems are the classical paraxial conditions of Clayton and Engquist (1977), high order non-reflecting conditions (*e.g.*, Givoli, 2004) and the Perfectly Matched Layer (PML) (Bérenger, 1994). In recent years the PML has become the preferred absorbing boundary for the elastic wave equation, due to its superior efficiency and flexibility when compared to other conditions such as, the Higdon paraxial condition. Despite the general success of the PML in most applications, there are still some instances for which the performance of the PML does not meet expectations. In the case of elastic waves in isotropic media, it has been reported (Festa *et al.*, 2005; Komatitsch and Martin, 2007) that large reflections are obtained for waves entering the PML at grazing incidence and also that instabilities appear in long (in time) simulations. In addition, Bécache *et al.*, (2003) documented that exponentially growing solutions could appear in some models for anisotropic media. Despite all the work done on the subject, a comprehensive mathematical analysis of the PML is not yet available and the problem of developing a general method to construct stable PML terminations remains open. In this thesis, the problem of stability and accuracy of the classical PML is studied. Motivated by these problems associated with PML, we have proposed (Meza-Fajardo, 2007; Meza-Fajardo and Papageorgiou, 2008) a new absorbing medium (referred to as the ***M**ulti-axial **P**erfectly **M**atched **L**ayer*, ***M-PML***) by generalizing the classical PML to a material for which damping profiles are specified in more than one direction.

It is the purpose of this short paper to sketch the formulation of the SEM in matrix form that is familiar to earthquake engineers. Detailed derivations may be found in Meza-Fajardo (2007).

## 2. MATHEMATICAL FORMULATION

For the problem of propagation of seismic waves through a region of the earth, seismologists usually model the medium of propagation as an elastic volume. The phenomena is then described by (i) the *momentum equation*, which is a statement of dynamic equilibrium, and (ii) the relation between displacements and forces, the well-known *generalized Hooke's law*. In variational methods of discretization such as the FEM, the resulting PDE is transformed into an integral equation, known as the *weak form*. After appropriate domain decomposition has been defined, the field variables are approximated and evaluated over the each sub-domain. The contributions of each sub-domain to inertial, external and internal forces are then assembled into a "global" system of ordinary differential equations of first order, which should then be discretized in time. The main ideas and results have been already presented in the papers by Komatitsch and Vilotte (1998) and Komatitsch and Tromp (1999) (see also Schuberth, 2003, for a tutorial exposition of the 1-D case).

The elastodynamics initial value problem is defined by Cauchy's equation of motion (also referred to as momentum equation):

$$\rho\ddot{\mathbf{u}} = \nabla \cdot \mathbf{T} + \mathbf{f} \tag{2.1}$$

with initial conditions:

$$\boldsymbol{u}_0(\mathbf{x}) = \mathbf{u}(\mathbf{x}, 0) \qquad \dot{\mathbf{u}}_0(\mathbf{x}) = \dot{\mathbf{u}}(\mathbf{x}, 0) \tag{2.2}$$

where $\mathbf{u}(\mathbf{x},t)$ is the displacement field, $\mathbf{x}$ is the position vector, $\mathbf{T}(\mathbf{x},t)$ is the stress tensor, $\rho(\mathbf{x})$ is the mass density, and the vector $\mathbf{f}(\mathbf{x},t)$ is a generalized body force.

The generalized Hooke's law may be expressed as follows:

$$\mathbf{T} = \mathbf{C} : \nabla\mathbf{u} \tag{2.3}$$

where $\mathbf{C}$ is the fourth-order tensor of elasticity and $\nabla\mathbf{u}$ denotes the tensor of the displacement gradient (Malvern, 1969).

Seismic sources can effectively be represented by and equivalent body force:

$$\mathbf{f} = -\boldsymbol{\nabla}\cdot\mathbf{m} \tag{2.4}$$

where $\mathbf{m}$ are is called the *moment density tensor*. The equivalent body force for a *tangential (i.e. shear) displacement dislocation* is given by $\mathbf{f} = -M_0(\mathbf{en}+\mathbf{ne})\cdot\delta(\mathbf{x}-\mathbf{x}_S)$ where $M_0$ is the (scalar) *seismic moment*; $\mathbf{e}$ is the unit vector defining the *direction of slip*; and $\mathbf{n}$ is the unit vector *normal to the plane of slip* (dyadic notation is used). The equivalent body force for a *center of compression* or *explosion* is represented by three dipoles of equal strength that are acting along three mutually perpendicular directions, and is represented as $\mathbf{f} = M_0\mathbf{e}_i\mathbf{e}_i$.

In order to discretize the equation of motion in the SEM, we use its weak (integral form). The equation of motion is multiplied by a time-independent generic weighting function (variation) $\boldsymbol{w}$, and the product is integrated over the spatial domain □ of the problem. After some algebraic manipulation, application of the divergence theorem and imposing the boundary conditions we obtain:

$$\int_\Omega \mathbf{w}\cdot\rho\frac{\partial^2\mathbf{u}}{\partial t^2}d\Omega = -\int_\Omega \tilde{\mathbf{T}}(\mathbf{u}):\nabla\mathbf{w}\,d\Omega + \int_\Omega \mathbf{w}\cdot\mathbf{f}\,d\Omega \tag{2.5}$$

A set of rectangular Cartesian axes $(x,y,z)$ is selected and the physical domain is divided into $N_e$ non-overlapping elements. Then the three integrals of the weak form (above) are evaluated separately for every element domain $\Omega_e$. For 3-D problems, the discretization using the SEM is restricted to hexahedral elements. In the case of 2-D problems, the elements are quadrilateral. The sides of the 3-D hexahedral elements as well as the 2-D quadrilateral elements are *isomorphous* to the square. Hence, there exists a unique mapping from the square to each quadrilateral element. The reference or *parent* element is defined in terms of coordinates $-1\le\xi\le+1$ , $-1\le\eta\le+1$ , $-1\le\zeta\le+1$ , which are referred to as the *local* or *natural coordinates*. The parent element of simple geometric shape is then mapped into distorted shapes in the global Cartesian coordinate system. The mapping is defined in terms of a set of *shape functions* $N_a(\xi,\eta,\zeta)$, and a set of $n_a$ *control* or *anchor nodes* $\mathbf{x}_a = \mathbf{x}(\xi_a,\eta_a,\zeta_a)$, $a=1,\cdots,n_a$, which define the geometry of the element. Points on the two domains (*i.e.*, the parent and physical domains) are then related as follows: $x(\xi,\eta,\zeta)=\sum_{a=1}^{n_a}N_a(\xi,\eta,\zeta)x_a$ , $y(\xi,\eta,\zeta)=\sum_{a=1}^{n_a}N_a(\xi,\eta,\zeta)y_a$ , $z(\xi,\eta,\zeta)=\sum_{a=1}^{n_a}N_a(\xi,\eta,\zeta)z_a$ . The derivatives that appear in the abovementioned integrals are easily converted from one coordinate system to another by means of the chain rule of partial differentiation. This operation introduces the *Jacobian* matrix, the determinant $J$ of which must be evaluated as well because it is used in the transformed integrals as follows: $\iiint dxdydz = \iiint Jd\xi d\eta d\zeta$ .

As just described, the shape of the boundary and volume elements can be defined in terms of low-degree Lagrange polynomials. In a traditional FEM, low-degree polynomials are also used as basis-functions for the representation of fields on the elements. In a SEM, on the other hand, a higher-degree *Lagrange interpolant* is used to express functions on the elements. Therefore, spectral elements are *subparametric*, because the interpolant used to describe the geometry is of lower order than the interpolant used to define the field variable. A scalar function $f$

(representing a field variable such as a displacement component) on a parent element $\Omega_e$ is interpolated by products of Lagrange polynomials of degree $N$ as:
$f(\mathbf{x}(\xi,\eta,\zeta)) = \sum_{i,j,k=0}^{N} l_i(\xi)\, l_j(\eta) l_k(\zeta) f^{ijk}$ , where $l_i(\xi)$ , $l_j(\eta)$ , $l_k(\zeta)$ are Lagrange polynomials of degree $N$, known as *cardinal functions*, that satisfy the condition $l_i(\xi_j) = \delta_{ij}$ ($\delta_{ij}$ = Kronecker delta), and $f^{ijk} = f\left(\mathbf{x}(\xi_i,\eta_j,\zeta_k)\right)$. In a SEM the control points $\xi_i$, $i = 1,\ldots,N+1$, needed in the definition of the Lagrange polynomials of degree $N$ are selected to be the $(N+1)$ *Gauss-Lobatto-Legendre* (*GLL*) points, which are the roots of the following equation: $(1-\xi^2)\frac{dL_N(\xi)}{d\xi} = 0$ , where $L_N$ denotes the *Legendre polynomial* of degree $N$. One can demonstrate that, for $N \geq 2$ , this equation has $N+1$ different real zeroes in the interval $[-1,+1]$ , the first and the last ones being $\xi_0 = -1$ and $\xi_N = +1$. Therefore, in a SEM some points always lie exactly on the boundaries of the elements. This choice of interpolation points is convenient because it allows one to enforce continuity of vector fields across the element boundaries. For wave propagation problems using a SEM one typically uses a polynomial degree $N$ between 5 and 10 to represent a function on the element.

A convenient *vectorial* representation of the values of a (scalar) field variable $f$ at the GLL points is given by (*e.g.*, Deville *et al.*, 2002):$\mathbf{f} = \left[f^1, f^2, \cdots, f^r, \cdots, f^{\mathcal{N}}\right]^T = \left[f^{000}, f^{100}, \cdots, f^{ijk}, \cdots, f^{NNN}\right]^T$, where $\mathcal{N} = (N+1)^3$ is the total number of nodal values in an element and the mapping $m = 1 + i + (N+1)j + (N+1)^2 k$ , translates the *three-index coefficient representation* $f^{ijk}$ to standard vector form $f^m$, with the first index advancing more rapidly. To illustrate the index mapping, the configuration for a 2-D parent element with interpolants of degree four is given in Figure 1:

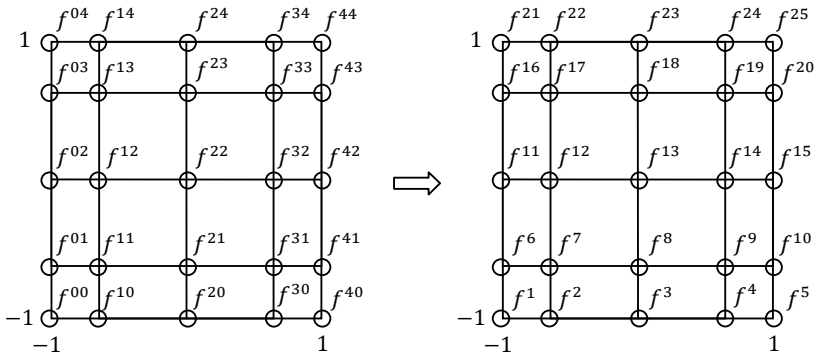

Figure 1: Index mapping to translate the two-index coefficient representation to standard vector form.

Values of the derivatives (with respect to the local coordinates) of the field variable $f$, evaluated at all the GLL points, may be organized in matrix form by using the ***tensor product*** (Meyer, 2000) as follows:

$$\left.\frac{\partial f}{\partial \xi}\right|_{\{\boldsymbol{\xi}\}} = \mathbf{D}_\xi \mathbf{f} \quad , \quad \left.\frac{\partial f}{\partial \eta}\right|_{\{\boldsymbol{\xi}\}} = \mathbf{D}_\eta \mathbf{f} \quad , \quad \left.\frac{\partial f}{\partial \zeta}\right|_{\{\boldsymbol{\xi}\}} = \mathbf{D}_\zeta \mathbf{f} \tag{2.6}$$

where: $\mathbf{D}_\xi = \mathbf{I}_{(N+1)} \otimes \mathbf{I}_{(N+1)} \otimes \mathbf{D}$ , $\mathbf{D}_\eta = \mathbf{I}_{(N+1)} \otimes \mathbf{D} \otimes \mathbf{I}_{(N+1)}$ , $\mathbf{D}_\zeta = \mathbf{D} \otimes \mathbf{I}_{(N+1)} \otimes \mathbf{I}_{(N+1)}$
$\mathbf{D} = [D_{pq}] = \left[\left(dl_q(\xi)/d\xi\right)\big|_{\xi=\xi_p}\right]$ is the $(N+1)\times(N+1)$ *one-dimensional derivative matrix*, and finally, the subscript $\{\boldsymbol{\xi}\}$ denotes *all* the GLL points. [Orszag (1980) pointed out early on that tensor-product forms were the foundation for efficient implementation of spectral methods.]

Let $\mathbf{u}_d = \left[u_d^1, u_d^2, \cdots, u_d^r, \cdots, u_d^{\mathcal{N}}\right]^T = \left[u_d^{000}, u_d^{100}, \cdots, u_d^{ijk}, \cdots, u_d^{NNN}\right]^T$, $d = x,y,z$ the vectorial representation of component $d\ (= x,y,z)$ of nodal displacements. Then the nodal values of the displacement field over the element may be represented as $\mathbf{U}^e = \left[\mathbf{u}_x, \mathbf{u}_y, \mathbf{u}_z\right]^T$. Then, the element mass matrix $\mathbf{M}^e$ can be expressed by means of the tensor product as:

$$\mathbf{M}^e = \mathbf{I}_D \otimes \widehat{\mathbf{M}}^e \tag{2.7}$$

where $\mathbf{I}_D$ is the $D \times D$ identity matrix, $D$ is the number of degrees of freedom per node (in the there-dimensional case $D = 3$). Denoting by $\omega^{ijk} = \omega_i \omega_j \omega_k$ the product of the weights of the GLL quadrature, the matrix $\widehat{\mathbf{M}}^e$ associated with each vector $\mathbf{u}_d$ is a diagonal matrix $\widehat{\mathbf{M}}^e = \text{diag}\left[\omega^{ijk} J^{ijk} \rho^{ijk}\right]$ .

The element stiffness matrix $\mathbf{K}^e$ takes the following form (for details of the derivation see Meza-Fajardo, 2007):

$$\mathbf{K}^e = \widehat{\mathbf{D}}_{\mathbf{x}}^T (\mathbf{C} \otimes \boldsymbol{\Omega}) \widehat{\mathbf{D}}_{\mathbf{x}} \tag{2.8}$$

where $\widehat{\mathbf{D}}_{\mathbf{x}} = (\mathbf{I}_3 \otimes \mathbf{J}^e)\widehat{\mathbf{D}}_{\boldsymbol{\xi}}$ , $\mathbf{I}_3$ is the $3 \times 3$ identity matrix, $\mathbf{J}^e$ is a $3\mathcal{N} \times 3\mathcal{N}$ matrix expressed as

$$\mathbf{J}^e = \begin{bmatrix} \mathbf{J}_{\xi,x} & \mathbf{J}_{\eta,x} & \mathbf{J}_{\zeta,x} \\ \mathbf{J}_{\xi,y} & \mathbf{J}_{\eta,y} & \mathbf{J}_{\zeta,y} \\ \mathbf{J}_{\xi,z} & \mathbf{J}_{\eta,z} & \mathbf{J}_{\zeta,z} \end{bmatrix}_{(3\mathcal{N}\times 3\mathcal{N})} \quad \text{and} \quad \widehat{\mathbf{D}}_{\boldsymbol{\xi}} = \begin{bmatrix} \mathbf{D}_\xi & \mathbf{D}_\eta & \mathbf{D}_\zeta & 0 & 0 & 0 & 0 & 0 & 0 \\ 0 & 0 & 0 & \mathbf{D}_\xi & \mathbf{D}_\eta & \mathbf{D}_\zeta & 0 & 0 & 0 \\ 0 & 0 & 0 & 0 & 0 & 0 & \mathbf{D}_\xi & \mathbf{D}_\eta & \mathbf{D}_\zeta \end{bmatrix}^T \tag{2.9}$$

with $\mathbf{J}_{\xi,l} = \text{diag}\left[(\partial\xi/\partial x_l)^{ijk}\right]_{(\mathcal{N}\times\mathcal{N})}$ , $\mathbf{J}_{\eta,l} = \text{diag}\left[(\partial\eta/\partial x_l)^{ijk}\right]_{(\mathcal{N}\times\mathcal{N})}$ , $\mathbf{J}_{\zeta,l} = \text{diag}\left[(\partial\zeta/\partial x_l)^{ijk}\right]_{(\mathcal{N}\times\mathcal{N})}$ .

The elasticity tensor $\mathbf{C}$ is represented as a $9 \times 9$ matrix of elastic constants, and $\boldsymbol{\Omega} = \text{diag}\left[\omega^{ijk} J^{ijk}\right]_{(\mathcal{N}\times\mathcal{N})}$. Therefore, the vector of *internal* forces $\mathbf{F}^{int,e}$ of element $e$ is given as $\mathbf{F}^{int,e} = \mathbf{K}^e \mathbf{U}^e$.

The vector of *external* forces (*sources*) $\mathbf{F}^e$ of element $e$, representing a point source concentrated at $\boldsymbol{\xi}_s = (\xi_s, \eta_s, \zeta_s)$ with *source function* $S(t)$, is given by the following expression:

$$\mathbf{F}^e = S(t)\mathbf{D}_s^T (\mathbf{I}_3 \otimes \mathbf{J}_s^{-1})^T \bar{\mathbf{M}} \tag{2.10}$$

where $\bar{\mathbf{M}} = \left[M_{xx}, M_{xy}, M_{xz}, M_{yx}, M_{yy}, M_{yz}, M_{zx}, M_{zy}, M_{zz}\right]^T$, and

$$\mathbf{J}_s^{-1} = \begin{bmatrix} \frac{\partial\xi}{\partial x} & \frac{\partial\eta}{\partial x} & \frac{\partial\zeta}{\partial x} \\ \frac{\partial\xi}{\partial y} & \frac{\partial\eta}{\partial y} & \frac{\partial\zeta}{\partial y} \\ \frac{\partial\xi}{\partial z} & \frac{\partial\eta}{\partial z} & \frac{\partial\zeta}{\partial z} \end{bmatrix}_{\{\boldsymbol{\xi}_s\}}, \quad \widehat{\mathbf{D}}_s = \begin{bmatrix} \mathbf{D}_{\xi_s} & \mathbf{D}_{\eta_s} & \mathbf{D}_{\zeta_s} & 0 & 0 & 0 & 0 & 0 & 0 \\ 0 & 0 & 0 & \mathbf{D}_{\xi_s} & \mathbf{D}_{\eta_s} & \mathbf{D}_{\zeta_s} & 0 & 0 & 0 \\ 0 & 0 & 0 & 0 & 0 & 0 & \mathbf{D}_{\xi_s} & \mathbf{D}_{\eta_s} & \mathbf{D}_{\zeta_s} \end{bmatrix}^T \tag{2.11}$$

Matrices $\mathbf{D}_{\xi_s}$, $\mathbf{D}_{\eta_s}$ and $\mathbf{D}_{\zeta_s}$, are row matrices of length $\mathcal{N}$, computed in the following manner:

$$\begin{aligned} \mathbf{D}_{\xi_s} &= \mathbf{H}_{\xi_s} \otimes \mathbf{H}_{\xi_s} \otimes \mathbf{D}(\xi_s) \\ \mathbf{D}_{\eta_s} &= \mathbf{H}_{\eta_s} \otimes \mathbf{D}(\eta_s) \otimes \mathbf{H}_{\eta_s} \\ \mathbf{D}_{\zeta_s} &= \mathbf{D}(\zeta_s) \otimes \mathbf{H}_{\zeta_s} \otimes \mathbf{H}_{\zeta_s} \end{aligned} \tag{2.12}$$

where $\mathbf{D}(\xi_s)$, $\mathbf{D}(\eta_s)$ and $\mathbf{D}(\zeta_s)$ are the rows of the one-dimensional derivative $\mathbf{D}$ matrix corresponding to the $\xi_s$, $\eta_s$, and $\zeta_s$ local coordinates, respectively. Finally, $\mathbf{H}_{\xi_s}$, $\mathbf{H}_{\eta_s}$ and $\mathbf{H}_{\zeta_s}$, are row vectors of length $(N+1)$ with only one non-zero entry, which also corresponds to the $\xi_s$, $\eta_s$, and $\zeta_s$ coordinates, respectively.

Assembling the above matrices and vectors, evaluated at the element level, into a *global mass matrix* $\mathbb{M} = \mathcal{A}_{e=1}^{N_e}\{\mathbf{M}^e\}$, a *global vector of external forces* $\mathbb{F} = \mathcal{A}_{e=1}^{N_e}\{\mathbf{F}^e\}$, and a *global vector of internal forces* $\mathbb{F}^{int} = \mathcal{A}_{e=1}^{N_e}\{\mathbf{F}^{int,e}\}$, we may write the semi-discrete form of the equation of motion as follows:

$$\mathbb{M}\ddot{\mathbb{U}} = \mathbb{F} - \mathbb{F}^{int} \tag{2.13}$$

which can be solved with an appropriate time-stepping algorithm.

A similar (but by no means trivial) procedure is followed to discretize the PML's attached to the computational domain. Detailed derivations and computational algorithms may be found in Meza-Fajardo (2007).

## 3. NUMERICAL EXAMPLES

An important application of the SEM in engineering seismology is the simulation of propagation of surface waves in geological basins. Thus, the first problem we present is a line explosive source embedded in a 2D homogeneous isotropic elastic half space. The physical domain is bounded at the top by a stress-free surface, and on the other three sides by M-PML terminations with ratios of damping profiles equal to 0.1. The free surface condition was also imposed on the top edges of the vertical layers, whereas Dirichlet boundary conditions $\mathbf{v} = \mathbf{0}$ were specified at all other external boundaries of the three absorbing layers. The dimensions and properties of the media and discretization parameters are listed in Table 1. For the simulations, we selected quadratic damping profiles of the form $d_x = d_0(x/H)^2$, $d_y = d_0(y/H)^2$, where $H$ is the thickness of the absorbing termination strip and the parameter $d_0$ is the maximum value of the damping profile in the strip. The value for $d_0$ is given in the form $d_0 = A\, v_p/H$, with $A = 10$, and $v_p$ is the P-wave velocity.

Table 1. Properties and discretization parameters for simulation in isotropic half space.

| **Physical domain dimensions** | | | **Ricker wavelet parameters** | | |
|---|---|---|---|---|---|
| Length | 11 | km | Dominant frequency | 2.5 | Hz |
| Width | 4 | km | Onset time | 0.4 | s |
| **Physical domain properties** | | | **Discretization parameters** | | |
| Density | 2.7E+12 | kg/km$^3$ | Polynomial degree | 8 | |
| S-wave velocity | 2.87 | km/s | Element side | 0.1 | km |
| P-wave velocity | 3.2 | km/s | Elements along PML width | 10 | |
| **Source location** | | | Time step | 0.00047 | s |
| From left boundary | 0.25 | km | Total duration | 8.5 | s |
| From bottom boundary | 0.85 | km | | | |

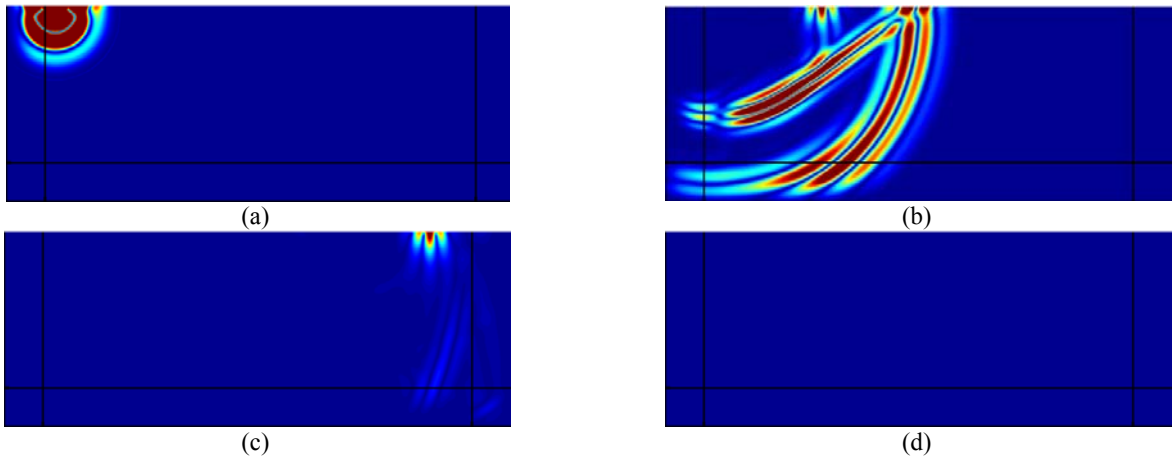

(a) (b) (c) (d)

Figure 1. Snapshots of propagation of velocity magnitude in an isotropic elastic medium with M-PML terminations at (a) t=0.5 s, (b) t=2 s, (c) t=6 s, (d) t=8.5 s.

In Figure 1 snapshots of the results are displayed for different instants. The interfaces between the physical domain and absorbing layers are represented by the solid lines. At t = 2 s the Rayleigh (surface) wave can be clearly identified. As expected, the Rayleigh way continues its propagation through the physical domain without any attenuation. It can be also observed that all body and surface waves are well absorbed by the M-PML terminations. The simulation seems to be stable, and no noticeable reflections due to the absorbing boundaries are observed.

As a second experiment we consider an embedded explosive line source and propagation of the radiation through two isotropic half spaces. The physical domain is then truncated with four M-PMLs. The source time variation is again a Ricker wavelet, and the damping profiles are of the same form as those used in the previous example (with $A = 7.5$). Other details of the physical domain properties and discretization parameters are listed in Table 2.

Snapshots of the propagation of the velocity magnitude at different time instants are shown in Figure 5. The interfaces between the two half spaces and the absorbing boundary are indicated by the black, solid lines. At time t = 1 s the wave front has already crossed from the softer to the stiffer half-space, and at t = 2 s the wave front is distorted due to the reflections at the interface between the two half-spaces. At time t=3.8 s most of the radiated energy has already left the physical domain, entered into the right M-PML and no noticeable reflections are observed. As the snapshots show, the simulation evolves without noticeable instabilities or reflections due to the absorbing boundaries, and at t=7.5 s no energy is visible in the physical domain.

Table 2. Properties and discretization parameters for simulation with two isotropic half-spaces.

| **Upper half space dimensions** | | |
|---|---|---|
| Length | 11 | km |
| Width | 2 | km |
| **Upper half space properties** | | |
| Density | 2.7E+12 | kg/km$^3$ |
| S-wave velocity | 1.87 | km/s |
| P-wave velocity | 3.2 | km/s |
| **Lower half space dimensions** | | |
| Length | 11 | km |
| Width | 2 | km |
| **Lower half space properties** | | |
| Density | 2.7E+12 | kg/km$^3$ |
| S-wave velocity | 2.34 | km/s |
| P-wave velocity | 4 | km/s |

| **Source location** | | |
|---|---|---|
| From left boundary | 0.5 | km |
| From bottom boundary | 3.5 | km |
| **Ricker wavelet parameters** | | |
| Dominant frequency | 2.5 | Hz |
| Onset time | 0.4 | s |
| **Discretization parameters** | | |
| Polynomial degree | 8 | |
| Element side | 0.1 | km |
| Elements along PML width | 7 | |
| Time step | 0.00047 | s |
| Total duration | 7.5 | s |

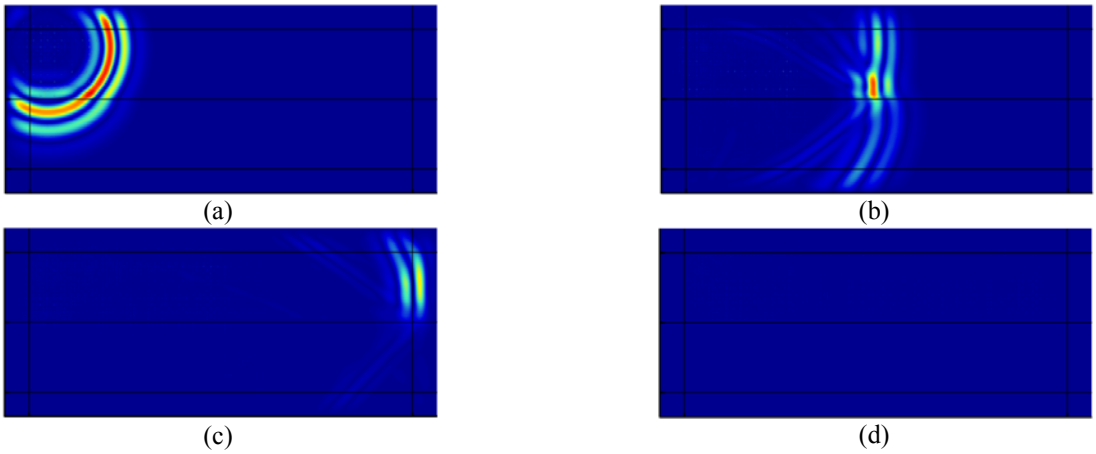

Figure 2. Snapshots of propagation of velocity magnitude in two isotropic elastic half-spaces with M-PML terminations at (a) t=1 s, (b) t=2 s, (c) t=3.8 s, (d) t=7.5 s.

## REFERENCES

Bécache, E., Fauqueux, S., Joly, P. (2003). Stability of perfectly matched layers, group velocities and anisotropic waves, *Journal of Computational Physics*, **188**, 399-433.

Bérenger, J.P. (1994). A Perfectly Matched Layer for the absorption of electromagnetic waves, *Journal of Computational Physics*, **114**, 185-200.

Clayton, R., Engquist, B. (1977). Absorbing boundary conditions for acoustic and elastic wave equations, *Bulletin of the Seismological Society of America,* **67**, 1529-1540.

Deville, M.O., Fischer, P.F., Mund, E.H. (2002). *High-order methods for incompressible fluid flow*, Cambridge University Press, Cambridge, UK.

Festa, G., Delavaud, E., Vilotte, J.P. (2005). Interaction between surface waves and absorbing boundaries for wave propagation in geological basins: 2D numerical simulations, *Geophysical Research Letters,* **32**, L20306, doi:10.1029/2005GL024091.

Givoli, D. (2004). High-order local non-reflecting boundary condition: a review, *Wave Motion,* **39**, 319-326.

Komatitsch, D., (1997). Méthodes spectrales et elements spectraux pour l'équation de l'élastodynamics 2D et 3D en milieu hétérogène (Spectral and spectral-element methods for the 2D and 3D elastodynamics equations in heterogeneous media), *PhD Thesis*, Institut de Physique du Globe, Paris, France.

Komatitsch, D., Vilotte, J.P. (1998). The spectral element method, *Geophysical Journal International*, **154**, 146-153.

Komatitsch, D., Tromp J. (1999). Introduction to the spectral element method for three-dimensional seismic wave propagation, *Geophysical Journal International*, **139**, 806-822.

Komatitsch, D., Martin R. (2007). As unsplit convolutional Perfectly Matched Layer improved at grazing incidence for the seismic wave equation, *Geophysics*, **72:5**, SM155-SM167.

Maday, Y., Patera, A.T. (1989). Spectral element methods for the incompressible Navier-Stokes equations, in: A.K. Noor (Editor), *State-of-the-Art Surveys in Computational Mechanics*, ASME, New York, 71-143.

Malvern, L.E., (1969). Introduction to the Mechanics of a Continuous Medium, Prentice-Hall Inc., New Jersey, USA.

Meyer, C.D. (2000). *Matrix Analysis and Applied Linear Algebra*, Society for Industrial and Applied Mathematics (SIAM), Philadelphia.

Meza-Fajardo, K.-C. (2007). Numerical Simulation of Wave Propagation in Unbounded Elastic Domains using the Spectral Element Method, *PhD Thesis*, Università degli Studi di Pavia, ROSE School, Pavia, Italy.

Meza-Fajardo, K.-C. and A.S. Papageorgiou (2008). A Non-Convolutional, Split-Field Perfectly Matched Layer (PML) For Wave Propagation In Isotropic And Anisotropic Elastic Media - Stability Analysis, *Bulletin of the Seismological Society of America*, **98:4**, (to appear).

Orzag, S.A. (1980). Spectral element methods for problems in complex geometries, *Journal of Computational Physics*, **37**, 70-92.

Patera, A.T. (1984). A Spectral element method for fluid dynamics: laminar flow in a channel expansion, *Journal of Computational Physics*, **54**, 468-488.

Schuberth B. (2003). The Spectral Element Method for Seismic Wave Propagation. Theory, implementation and comparison to Finite Difference Methods, *Diploma Thesis,* Dept. for Earth and Environmental Sciences, Ludwig-Maximilians-Universität München.